

Electronic Supplementary Material (ESI) for Journal of Materials Chemistry C.

Electronic Supporting Information

Water-enhanced high-efficiency persistent room-temperature phosphorescence materials for temperature sensing via crystalline transformation

Xuwei Luo^a, Lifen Chen^a, Bo Liu^a, Zhiwen Yang^a, Longmeng Wei^b, Zhanxiang Yuan^a, Yudong Wen^a, Yingxiao Mu^{*a}, Yanping Huo^a, Hao-Li Zhang^{*ac} and Shaomin Ji^{*a}

^a School of Chemical Engineering and Light Industry, Guangdong University of Technology, Guangzhou 510006, PR China

E-mail: yxmu@gdut.edu.cn (Y. Mu), haoli.zhang@lzu.edu.cn (H.-L. Zhang), smji@gdut.edu.cn (S. Ji)

^b Analysis and Test Center, School of Environmental Science and Engineering, Guangdong University of Technology, Guangzhou 510006, PR China

^c State Key Laboratory of Applied Organic Chemistry, Key Laboratory of Special Function Materials and Structure Design, College of Chemistry and Chemical Engineering, Lanzhou University, Lanzhou 730000, PR China

Experimental Section

Reagents and materials

All the reagents and solvents were purchased from commercial suppliers and purified by column chromatography once.

Measurements

^1H NMR spectra were recorded on a Bruker AV 400 spectrometer. High-resolution mass spectra (LC-MS) were recorded using a GCT premier TSQ Endura mass spectrometer, operating in a Thermo Fisher TSQ EnduraTM Mass spectrometer. Ultraviolet-visible absorption spectra of the samples were recorded using Shimadzu UV-2700 UV-vis Spectrophotometer. Steady-state photoluminescence (PL) and transient PL spectra were measured using the Edinburgh FLS980 spectrometer under ambient condition. The phosphorescence spectra were studied by a multi-function spectrometer (HPX-200C-HP- DUV).

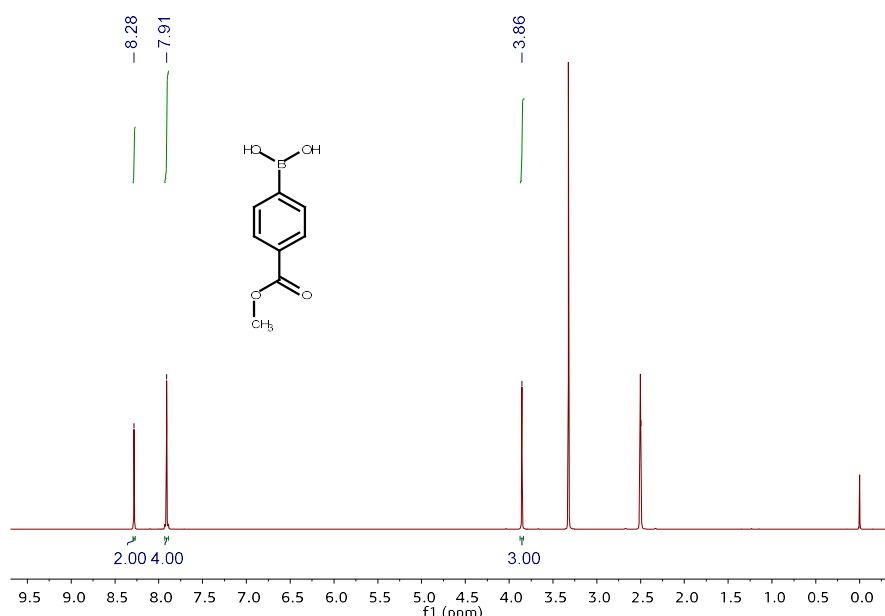


Fig. S1. ^1H NMR spectrum of MP in d-DMSO.

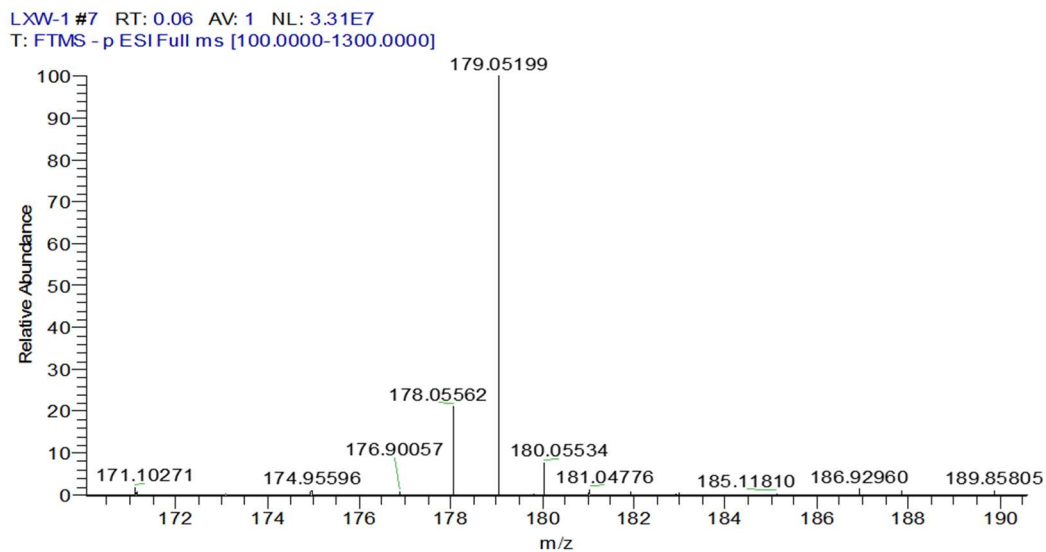


Fig. S2. Mass spectrum of MP.

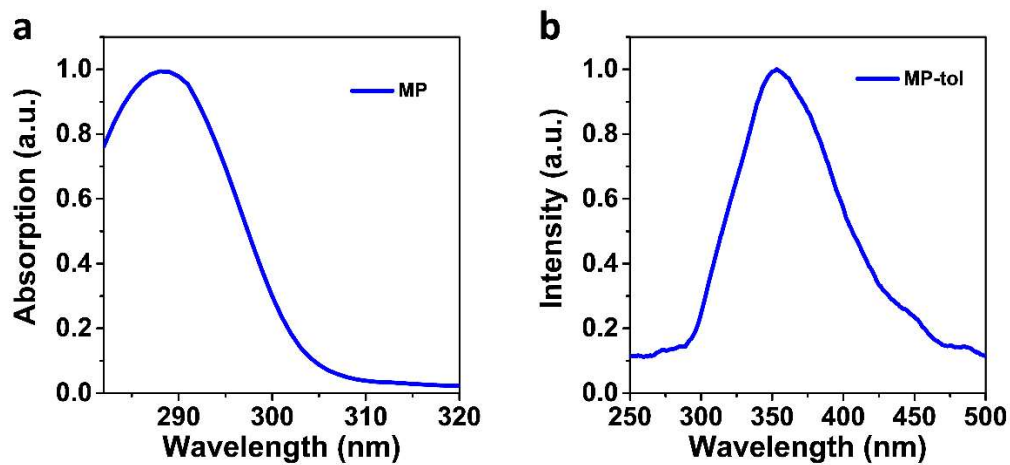


Fig. S3. Normalized (a) UV-Vis absorption and (b) steady-state PL spectra of MP in toluene under ambient conditions (Concentration: 10^{-5} M).

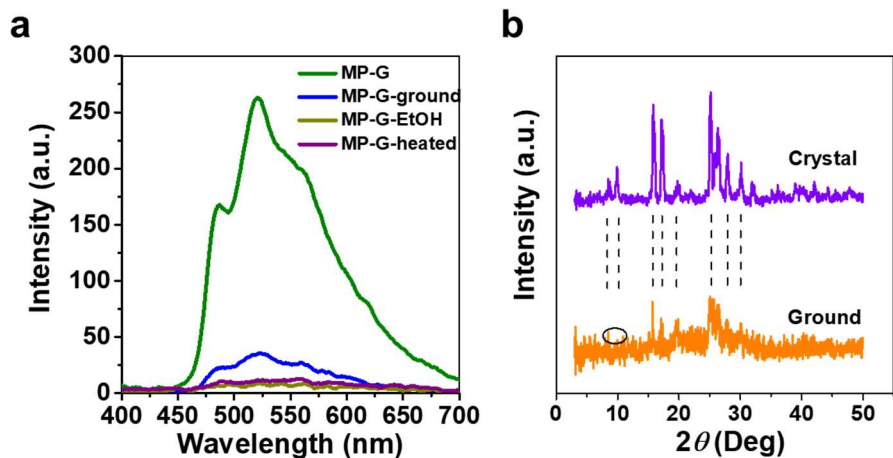


Fig. S4. (a) Delay spectra of MP-G after grinding, heating, and fuming with ethanol (EtOH), respectively. (b) Powder XRD patterns of MP-G in different states.

Table S1. Summary of the crystal data for MP, MP-G and MP-B.

Identification code	MP	MP-G	MP-B
Empirical formula	C ₈ H ₉ BO ₄	C ₈ H ₁₁ BO ₅	C ₈ H ₁₁ BO ₅
Formula weight	179.96	197.98	197.98
Temperature/K	230 K	298 K	150 K
Crystal system	monoclinic	triclinic	triclinic
Space group	P21/c	P-1	P-1
a/Å	5.9989(3)	8.6172(3)	8.6172(3)
b/Å	21.9945(11)	10.4308(4)	10.4308(4)
c/Å	7.0571(3)	12.1320(5)	12.1320(5)
α/°	90°	72.103(2)°	72.103(2)°
β/°	100.832(2)°	75.725(2)°	75.725(2)°
γ/°	90°	74.526(2)°	74.526(2)°
Volume/Å ³	914.54(8)	983.86(7)	983.86(7)
Z	4	4	4
Dx,g cm ⁻³	1.307	1.337	1.337
μ/mm-1	0.102	0.109	0.109
F(000)	376.0	416.0	416.0
Radiation	Mo	Mo	Mo
R1 (I>2σ(I))	0.0381	0.0576	0.0576
wR2 (I>2σ(I))	0.1154	0.1706	0.1706
CCDC number	2106216	2106218	2143084

Table S2. Types and distances of intermolecular interactions in MP, MP-G and MP-B crystals.

MP		MP-G		MP-B	
Types of bond	distance (Å)	Types of bond	distance (Å)	Types of bond	distance (Å)
O-H···B	2.962	O-H···B	2.794	O-H···B	2.917
	3.510		2.932		2.948
			3.417		1.931
O-H···O	1.934	O-H···O	1.875	O-H···O	1.919
			1.911		2.056
			1.993		1.919
O-H···C	3.048	B-O···O-H	2.611	B-O···O-H	2.056
			2.691		2.640
			2.297		2.546
C-H···B	3.079 3.573	O-H···H	2.423	O-H···H	2.389
			2.333		2.355
			2.433		2.423
C···B-O	3.519	C-H···H	2.628	C-H···H	2.475
			2.782		2.541
			2.922		2.767
C-O···B	3.336 3.363	C-H···O-H	2.702	C-H···O-H	2.761
			2.591		2.847
			2.618		2.502
C=O···O-B	2.752 1.973	C-O···B	2.800	C-H···O-H	2.530
			2.915		2.843
			3.401		--
C=O···H	2.585 3.039	C-H···B	3.208	C-H···B	3.168
					3.378
C-H···H	2.555 2.857	O-H···C	2.845	O-H···C	2.502
					2.517
					2.530

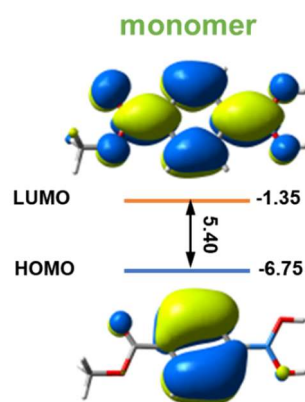


Fig. S5. The calculated highest occupied molecular orbital (HOMO) and lowest unoccupied molecular orbital (LUMO) energy levels of optimized MP monomer.

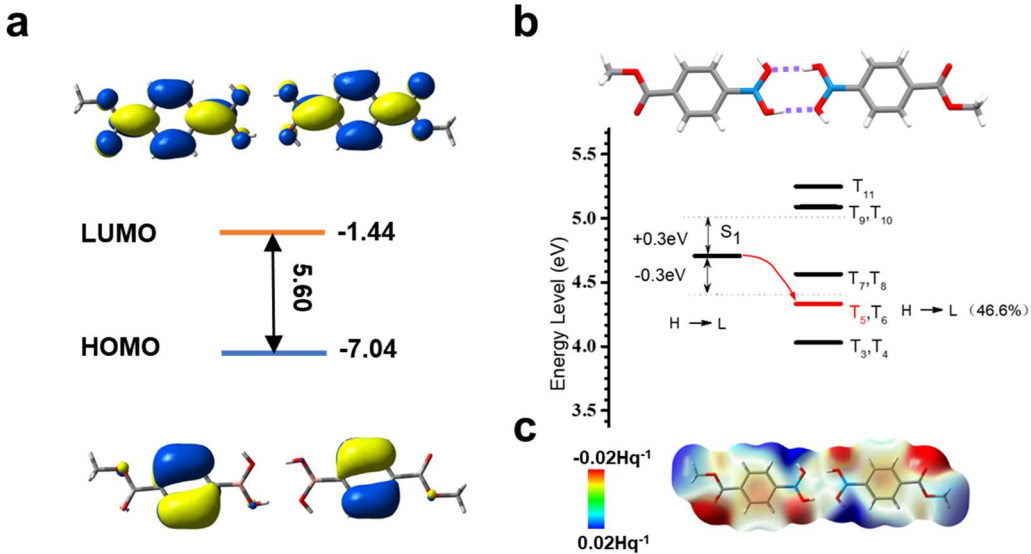


Fig. S6. The calculated highest occupied molecular orbital (HOMO) and lowest unoccupied molecular orbital (LUMO) energy levels of dimers based on MP crystals and the corresponding energy gaps. (b) The energy level diagrams of the dimer. (c) The calculated electrostatic potential (ESP) maps of dimer based on MP crystals.

Table S3. The singlet and triplet excited states transition configurations of MP dimer revealed by TD-DFT calculations. The matched excited states that contain the same orbital transition components of S_1 were highlighted in red.

n-th	Energy (eV)	Transition configuration (%)
S_n	1	4.7072 H-4→L (46%), H-4→L+1(42.3%), H-4→L+4(2%)
T_n	1	3.4646 H-3→L (11.5%), H-3→L+1 (27.4%), H-2→L (27.3%), H-2→L+1(2.3%), H-1→L (3.4%), H-1→L+2 (4%), H-1→L+3 (4.6%), H→L+2 (3.3%),
	2	3.4647 H-3→L (27.8%), H-3→L (11.5%), H-2→L (9.7%), H-2→L+1(26%), H-1→L+2 (4.9%), H→L+2 (3.4%), H→L+3 (5%)
3	4.0293	H-1→L (27.4%), H-1→L+1 (28%), H→L (19.2%), H→L+1 (32%)
4	4.0294	H-1→L (22%), H-1→L+1 (23.5%), H→L (28.7%), H→L+1 (34%)
5	4.3330	H-4→L (46.1%), H-4→L+1 (44.2%), H-4→L+4 (3.9%), H-4→L+5 (3.5%)
6	4.3336	H-5→L (44.6%), H-5→L+1 (46.8%), H-5→L+4 (3.7%), H-5→L+5 (3.9%)
7	4.5651	H-3→L (2.8%), H-3→L+1 (3.3%), H-2→L(7%), H-2→L+1(2.3%), H-1→L+2 (18%), H-1→L+3 (13%), H→L+2 (19.3%), H→L+3 (9%)
8	4.5652	H-3→L (5%), H-3→L+1 (3.6%), H-2→L(3%), H-2→L+1(4.8%), H-1→L+2 (26%), H-1→L+3 (9%), H→L+2 (16.8%), H→L+3(29%),
9	5.0895	H-7→L (8.8%), H-7→L+1 (9%), H-6→L (27.4%), H-6→L (26.7%), H-6→L+1 (29%), H-6→L+4 (9.8%), H-6→L+5 (11%),

Table S4. The singlet and triplet excited states transition configurations of MP-G dimer 1 revealed by TD-DFT calculations. The matched excited states that contain the same orbital transition components of S_1 were highlighted in red.

	n-th	Energy (eV)	Transition configuration (%)
S_n	1	3.9629	$H \rightarrow L$ (98%)
T_n	1	3.4666	$H-1 \rightarrow L+2$ (55.3%), $H-1 \rightarrow L+4$ (4.4%), $H \rightarrow L+2$ (25.7%), $H \rightarrow L+5$ (12.8%)
	2	3.4955	$H-4 \rightarrow L$ (67.3%), $H-3 \rightarrow L$ (12%), $H-3 \rightarrow L+1$ (22.6%)
	3	3.9628	$H \rightarrow L$ (98.9%)
	4	4.0067	$H-1 \rightarrow L$ (94%), $H \rightarrow L+2$ (13.9%)
	5	4.0148	$H-1 \rightarrow L$ (5.5%), $H-1 \rightarrow L+2$ (27.8%), $H \rightarrow L+2$ (63.4%)
	6	4.0407	$H-4 \rightarrow L$ (10%), $H-4 \rightarrow L+1$ (5.5%), $H-3 \rightarrow L$ (86.6%)

Table S5. The singlet and triplet excited states transition configurations of MP-G dimer 2 revealed by TD-DFT calculations. The matched excited states that contain the same orbital transition components of S_1 were highlighted in red.

	n-th	Energy (eV)	Transition configuration (%)
S_n	1	4.6090	$H-5 \rightarrow L$ (5%), $H \rightarrow L$ (92%)
T_n	1	3.4564	$H-1 \rightarrow L+1$ (64%), $H-1 \rightarrow L+3$ (2%), $H \rightarrow L+1$ (16%), $H \rightarrow L+3$ (14.7%),
	2	3.4975	$H-4 \rightarrow L$ (63.5%), $H-4 \rightarrow L+2$ (3.3%), $H-3 \rightarrow L$ (15.6%), $H-3 \rightarrow L+2$ (15%),
	3	3.9735	$H-1 \rightarrow L$ (17%), $H-1 \rightarrow L+1$ (2.2%), $H \rightarrow L+1$ (77.8%)
	4	4.0677	$H-4 \rightarrow L$ (18%), $H-4 \rightarrow L+2$ (2.7%), $H-3 \rightarrow L$ (65.7%), $H-2 \rightarrow L$ (13%)
	5	4.3098	$H-5 \rightarrow L$ (89.8%), $H-5 \rightarrow L+4$ (7.7%)
	6	4.4054	$H-3 \rightarrow L+1$ (4%), $H-2 \rightarrow L+1$ (81.4%), $H-2 \rightarrow L+5$ (8%)
	7	4.5222	$H-4 \rightarrow L$ (17.6%), $H-4 \rightarrow L+2$ (15.5%), $H-3 \rightarrow L$ (3.3%), $H-3 \rightarrow L+2$ (59.4%), $H-3 \rightarrow L+2$ (5%)
	8	4.5540	$H-1 \rightarrow L+1$ (12.5%), $H-1 \rightarrow L+3$ (8.7%), $H \rightarrow L$ (17.6%), $H \rightarrow L+3$ (57.5%)
	9	4.6410	$H \rightarrow L$ (79.8%), $H \rightarrow L+1$ (2%), $H \rightarrow L+3$ (6%)
	10	4.7246	$H-2 \rightarrow L$ (81.3%)
	11	5.0575	$H-7 \rightarrow L$ (74.6%), $H-7 \rightarrow L+4$ (8%), $H-4 \rightarrow L+3$ (7.4%)

Table S6. The singlet and triplet excited states transition configurations of MP-G dimer 3 revealed by TD-DFT calculations. The matched excited states that contain the same orbital transition components of S_1 were highlighted in red.

	n-th	Energy (eV)	Transition configuration (%)
S_n	1	4.5206	H-5→L (37%), H→L (54%)
T_n	1	3.4459	H-4→L+1 (3.8%), H-1→L (2.4%), H-1→L+1 (56.6%), H→L+1 (7.7%), H→L+3(14%)
	2	3.4958	H-4→L (59.3%), H-2→L+2 (18%), H-1→L (17.6%), H-1→L+1(2.4%)
	3	3.9695	H-1→L (6.7%), H-1→L+1 (3.5%), H→L+1 (75.6%)
	4	4.0934	H-4→L+2 (2.5%), H-3→L (4%), H-2→L (74.5%)
	5	4.2119	H-5→L (73%), H-5→L+4 (6%), H→L (6%)
	6	4.4430	H-3→L (2%), H-3→L+1 (72%), H-3→L+5 (9%), H-2→L+1 (8.7%), H→L+3 (2.6%)
	7	4.4739	H-4→L (3%), H-3→L+2 (2.7%), H-2→L+2(34%), H-1→L (28%), H→L (9%), H→L+2(2%), H→L+3 (3%)
	8	4.5218	H-4→L (3%), H-3→L+1 (3%), H-2→L+2(6%), H-1→L+1 (5.8%), H-1→L+3 (2%), H→L (18%), H→L+1(2%), H→L+3 (39%)
	9	4.6168	H-4→L (4%), H-1→L+1 (2.7%), H→L(59%), H-1→L+2 (2%), H→L+3 (19%)
	10	4.6987	H-4→L (21.3%), H-2→L (2.5%), H-2→L+2(3.4%), H-1→L (57%)
	11	4.9644	H-7→L (50%), H-7→L+4 (8%), H-6→L (29%), H-6→L+4 (2%), H-4→L+2 (2.4%), H→L (2%)

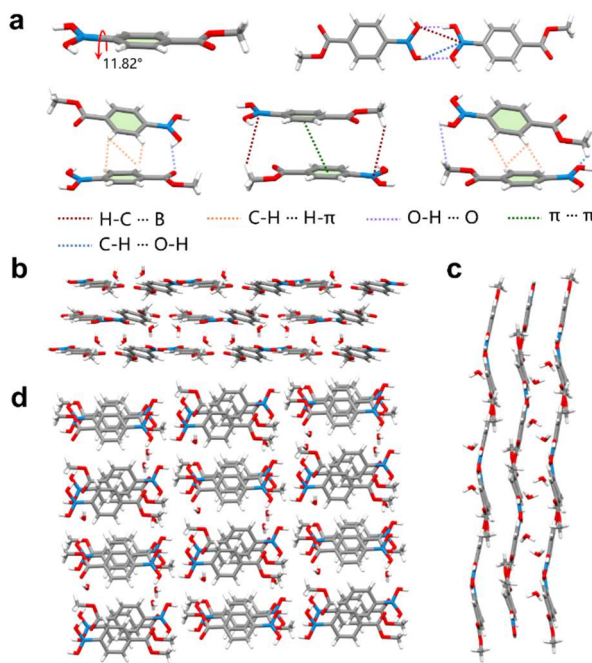


Fig. S7. Single crystal structure of MP-B. (a) Illustration of the torsion angle between the carboxyl group and benzene ring, molecular packing in dimer. Entire packing along the (b) front view, (c) side view and (d) top view.

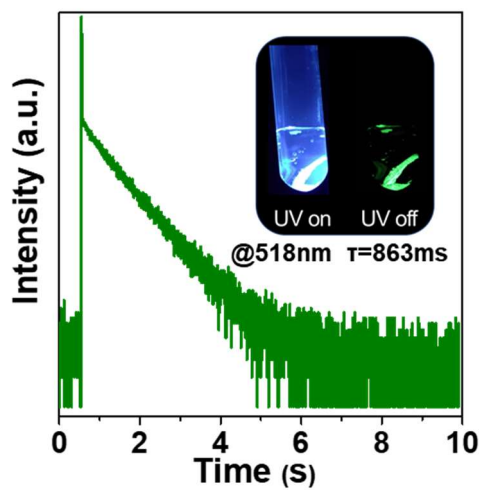


Fig. S8. Time-resolved PL decay curves of MP-G measured in aqueous solution at room temperature. Inset: photographs of MP-G crystal in aqueous solution before and after removal of UV lamp irradiation.